

PAPER

## Investigation of partitionless growth of $\epsilon\text{-Al}_{60}\text{Sm}_{11}$ phase in Al-10 at% Sm liquid

To cite this article: Yang Sun *et al* 2018 *Modelling Simul. Mater. Sci. Eng.* **26** 015006

View the [article online](#) for updates and enhancements.

# Investigation of partitionless growth of $\varepsilon$ -Al<sub>60</sub>Sm<sub>11</sub> phase in Al-10at% Sm liquid

Yang Sun<sup>1,2,4</sup> , Zhuo Ye<sup>1</sup>, Feng Zhang<sup>1</sup>, Ze Jun Ding<sup>2</sup>,  
Cai-Zhuang Wang<sup>1,3</sup> , Matthew J Kramer<sup>1</sup> and  
Kai-Ming Ho<sup>1,2,3,4</sup>

<sup>1</sup> Ames Laboratory, US Department of Energy, Ames, IA 50011, United States of America

<sup>2</sup> Hefei National Laboratory for Physical Sciences at the Microscale and Department of Physics, University of Science and Technology of China, Hefei, Anhui 230026, People's Republic of China

<sup>3</sup> Department of Physics, Iowa State University, Ames, IA 50011, United States of America

E-mail: [yangsun@ameslab.gov](mailto:yangsun@ameslab.gov) and [kmh@iastate.edu](mailto:kmh@iastate.edu)

Received 7 August 2017

Accepted for publication 31 October 2017

Published 7 December 2017



CrossMark

## Abstract

Recent experiments on devitrification of Al<sub>90</sub>Sm<sub>10</sub> amorphous alloys revealed an unusual polymorphic transformation to a complex cubic crystal structure called the  $\varepsilon$ -Al<sub>60</sub>Sm<sub>11</sub> phase. Molecular dynamics simulations of the growth of the stoichiometric  $\varepsilon$ -phase seed in contact with an undercooled Al-10 at% Sm liquid are performed to elucidate the microscopic process of transformation. The as-grown crystal and undercooled liquid possess similar local order around Al atoms whereas a rigid network defined by the Sm sub-lattice develops during the growth. Using a template-cluster alignment method, we define an order parameter to characterize the structural evolution in the system. Estimates of the attachment rate is  $R_a = 8.70 \times 10^{-4} \text{ \AA}^{-2} \text{ ns}^{-1}$  and detachment rate is  $R_d = 3.83 \times 10^{-4} \text{ \AA}^{-2} \text{ ns}^{-1}$  at the interface between  $\varepsilon$ -Al<sub>60</sub>Sm<sub>11</sub> and Al-10 at% Sm liquid at 800 K.

Keywords: molecular dynamics simulation, short-range order, solid-liquid interface

(Some figures may appear in colour only in the online journal)

<sup>4</sup> Authors to whom any correspondence should be addressed.

## 1. Introduction

Amorphous alloys can display a complicated devitrification behavior during heating [1, 2]. Phase and morphological selection is dependent on complex relationships between thermodynamic and kinetic factors, such as relative differences in free energy between competing phase, local chemical partitioning and epitaxial growth [3]. One approach is to search for relevant order parameters which describe this transformation, paving the way for a phase-field description which can enable detailed realistic simulations of the devitrification process. While thermodynamic measurements provide energetics of the phase transformation and *in situ* XRD studies can provide more detailed phase information [4], details of local atomic order during the transformation is challenging [5]. In this situation, atomistic simulation becomes a valuable tool to provide insight into the detailed atom-level processes [6].

The Al–Sm binary alloy is a prototype of marginal glass-forming system which exhibits the widest glass-forming composition range in the Al–RE (RE for rare earth element) series [7, 8]. It has been shown that the devitrification of the Al–Sm alloys within the glass formation composition range is a complicated process [9–12]. For the melt-spun ribbon sample of the Al<sub>90</sub>Sm<sub>10</sub> amorphous alloy, it shows a multi-step devitrification pathway from the glass state transforming to various metastable crystalline phases [11]. After holding the as-quenched Al<sub>90</sub>Sm<sub>10</sub> glass at 457 K for 10 min, crystal grains appear and continue to grow rapidly until the sample totally transforms into a single crystal phase in  $\sim 1$  h [13]. A recent study using the genetic algorithm and Rietveld refinement solved the crystal structure of the first phase that appears in this complicated process: the  $\epsilon$ -Al<sub>60</sub>Sm<sub>11</sub> phase [12]. It has a complex structure containing around 140 atoms in the unit cell. X-ray data and theoretical simulations both provide evidence that the experimentally grown crystal structure has further structural complexity in the form of abundant point defects [12].

Although it is difficult to directly simulate the growth of the  $\epsilon$ -Al<sub>60</sub>Sm<sub>11</sub> phase in the Al<sub>90</sub>Sm<sub>10</sub> glass due to the limitation of the short timescales ( $\leq \mu\text{s}$ ) in current molecular dynamics (MD) simulations, it is possible to extract information about the growth process in the undercooled liquid state using accelerated MD at an elevated temperature. The stoichiometric  $\epsilon$ -Al<sub>60</sub>Sm<sub>11</sub> with a surface termination (100) was placed in contact with the undercooled liquid of Al-10 at% Sm. The atomic cluster alignment method [14], which quantifies the structural deviation between an as-extracted cluster and the template motif, is employed to reveal the behavior of the local structural order during the growth. The interface velocity during growth can be derived from alignment analysis. By tracing the atomic motion, the dynamic pathway from the undercooled liquid to crystal is revealed. Frequent atom attachment and detachment are found at the solid–liquid interface. The estimated attachment and detachment rates are consistent with the interface velocity in our simulation.

## 2. MD simulations

The initial structure in the simulation is constructed by combining the stoichiometric  $\epsilon$ -Al<sub>60</sub>Sm<sub>11</sub> and the undercooled Al-10 at% Sm liquid. A supercell of the  $\epsilon$ -Al<sub>60</sub>Sm<sub>11</sub> containing 3834 atoms is placed at the left part of the simulation box. The Al-10 at% Sm liquid, containing 3840 atoms, is quenched from 2000 to 800 K and annealed at 800 K for 3 ns to get equilibrium. Then the liquid sample is placed at the right part of the simulation box adjacent to the (100) crystal plane of the  $\epsilon$ -Al<sub>60</sub>Sm<sub>11</sub>. The periodic boundary condition is applied in all three directions of the simulation box. All the simulations are performed with Nose–Hoover thermostats. During the simulation, we allow the length of the box in the direction

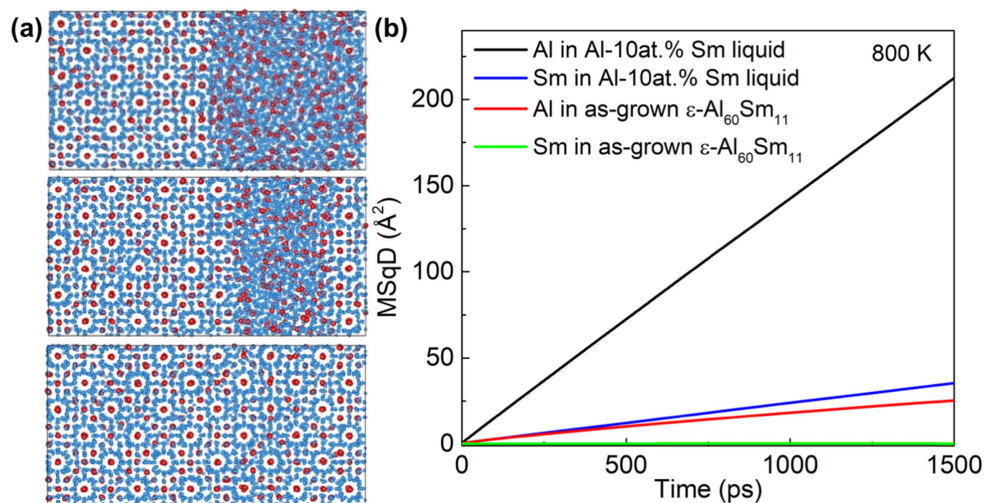


**Figure 1.** (a) The projected snapshots of the initial, medium and final configurations during simulation. The blue ball stands for Al atoms and red for Sm atoms. (b) The mean square displacement for Al and Sm atoms in initial liquid and the as-grown structure.

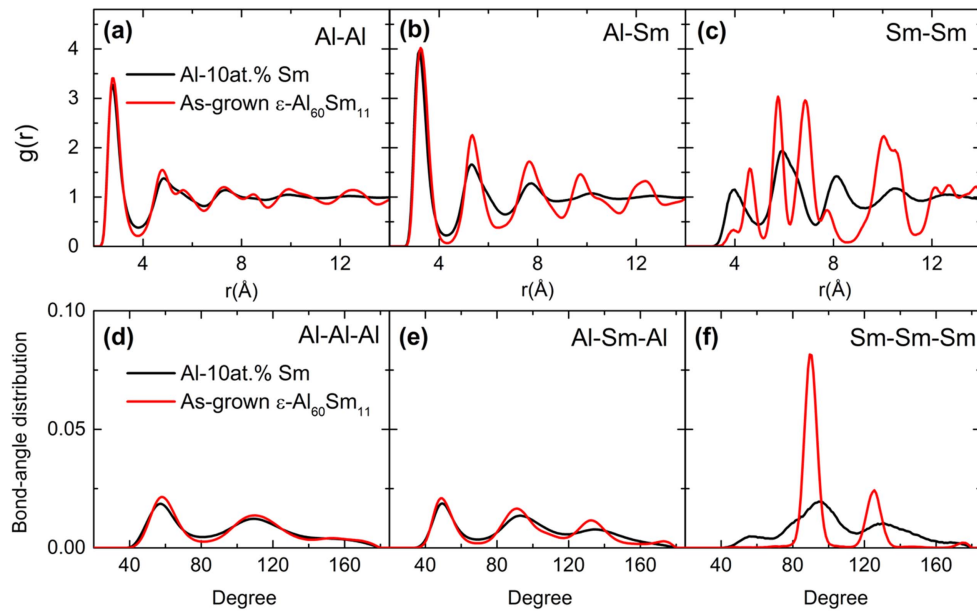
perpendicular to the interface to change, resulting in constant area, constant normal pressure:  $NP_xAT$  ensemble, with  $x$  being the perpendicular direction. The Verlet algorithm is used to integrate Newton's equation of motion, using a time step of 3 fs. The sample is annealed at 800 K for 285 ns that the Al-10 at% Sm undercooled liquid fully completes the transformation to the crystal structure. The simulations are performed with the Large-scale Atomic/Molecular Massively Parallel Simulator [15] using a semi-empirical Finnis-Sinclair potential for Al-Sm system [16].

Figure 1(a) shows the projected snapshots at the initial, medium and final time of the simulation, respectively. The total simulation time is 285 ns. One can see the growth of the  $\epsilon$  phase into the liquid. The mean square displacement is plotted as a function of time in figure 1(b). Both Al and Sm atoms' diffusion slow dramatically, indicating that the crystalline phase has consumed the liquid.

### 3. Results and discussions

#### 3.1. Pair correlation function (PCF) and bond angle distribution

In figures 2(a)–(c), the PCF are plotted for the Al-10 at% Sm undercooled liquid and the as-grown  $\epsilon$ -Al<sub>60</sub>Sm<sub>11</sub> structure. Compared to the liquid state, the PCF peaks of the as-grown structure are sharper and narrower, indicating strong crystalline order. However, the peaks in Al–Al and Al–Sm PCFs of the liquid and as-grown  $\epsilon$ -Al<sub>60</sub>Sm<sub>11</sub> show interesting coincidences in figures 2(a) and (b). Since the nearest neighbor atoms for both Al and Sm atoms are dominated by the Al atoms at the 10 at% Sm composition, such coincidence suggests that the local atomic arrangements of Al atoms are similar in the undercooled liquid and the crystal. In figure 2(c), the first peak of liquid Sm–Sm PCF at 3.9 Å dramatically decreases after the crystallization, while a new peak emerges at 4.6 Å, indicating the development of a Sm–Sm network during the crystallization [17].



**Figure 2.** The PCFs and bond angle distributions in the undercooled Al-10 at% Sm liquid and as-grown  $\varepsilon$ -Al<sub>60</sub>Sm<sub>11</sub> phase. (a) Al–Al PCF; (b) Al–Sm PCF; (c) Sm–Sm PCF; (d) Al–Al–Al angle distribution; (e) Al–Sm–Al angle distribution; (f) Sm–Sm–Sm angle distribution. The bond length cutoffs are chosen to be 3.8 Å for the Al–Al pair, 4.2 Å for the Al–Sm pair and 5.2 Å for the Sm–Sm pair according to the PCFs.

In addition to the PCFs, we performed bond angle analysis as shown in figures 2(d)–(f). In figure 2(d), the Al–Al–Al bond angle distribution in the liquid sample exhibits strong peaks at around 60° and 110° as well as a shoulder peak at 160°, which is similar to that of pure Al liquid [18]. After the liquid crystallizes, these angular distributions simply sharpen, indicating the Al packing is unaffected during the crystallization. In figure 2(e), the peaks of Al–Sm–Al bond angle distributions also narrow and sharpen during crystallization. However, in figure 2(f), the Sm–Sm–Sm bond angle distribution changes dramatically, with two sharp peaks emerging at 90° and 125°. Similar to the change of the Sm–Sm PCF in figure 2(c), the change in Sm–Sm–Sm bond angle distribution also indicates that the Sm–Sm packing undergoes dramatic reconstructed during crystallization.

### 3.2. Alignment analysis of atomic clusters

A comprehensive picture of the structural order requires not only bond length and bond angle distributions, but also an explicit identification of the local packing motif. While lacking long-range translational symmetry, the undercooled metallic liquids and glasses have clear elements of short- and medium-range order [6, 19–25]. Many studies have led to the conclusion that the solute-centered atomic clusters are representative structural elements and fundamental building block in metallic structures [6, 20, 26]. Therefore, we investigate the transformation of local order around the solute Sm atoms and its relationship to the crystallization process. A close inspection can find two types of Sm centered clusters in the  $\varepsilon$ -Al<sub>60</sub>Sm<sub>11</sub>, namely, 3661 and 16661 motifs [12] as shown in figures 3(a) and (b), respectively. Figure 3(c) shows the arrangement of two motifs in the crystal structure. The 3661 motif is also found to be

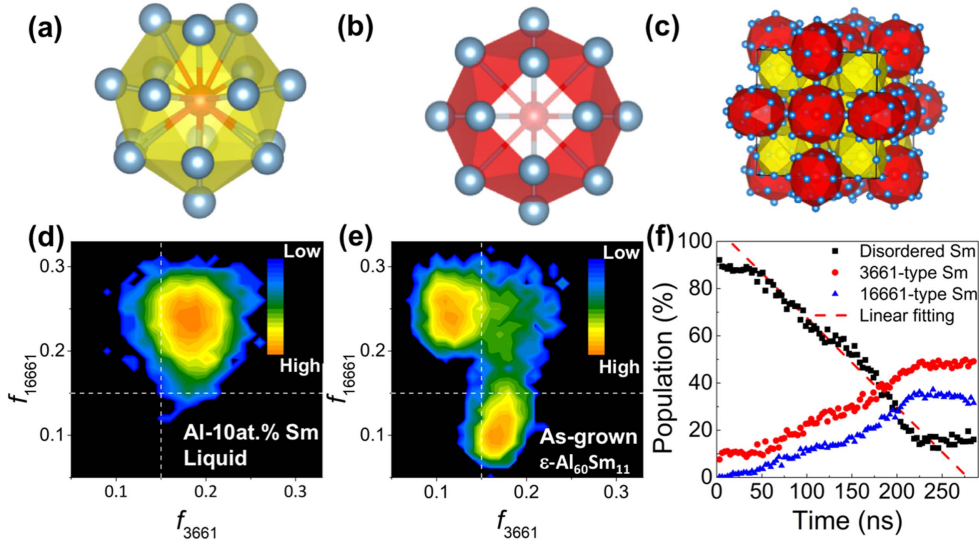


**Figure 3.** (a) 3661-type cluster. (b) 16661-type cluster. Red ball stands for Sm and blue for Al. (c) The arrangement of 3661-type clusters (yellow) and 16661-type clusters (red) in the  $\epsilon$ -Al<sub>60</sub>Sm<sub>11</sub> structure. (d) and (e) The  $(f_{3661}, f_{16661})$  score distribution of the Sm clusters from the liquid and as-grown  $\epsilon$ -Al<sub>60</sub>Sm<sub>11</sub> structure, respectively. The dash line indicates 0.15 as the threshold to classify the different types of clusters. (f) The population of 3661-type, 16661-type and disordered clusters as a function of simulation time. The linear fitting is used to estimate the interface velocity.

dominant in the Al-10 at% Sm liquid and glass [27, 28]. To understand how these motifs evolve during the crystallization, we employ the alignment analysis [27, 29] for Sm-centered clusters, using 3661 and 16661 motifs as templates following the individual template-cluster alignment procedure described in [14]. The alignment score, describing how an as-extracted cluster deviates from the perfect template, is defined as

$$f = \min_{\alpha} \sqrt{\frac{1}{N} \sum_{i=1}^N \frac{(\mathbf{r}_{ci} - \alpha \mathbf{r}_{ti})^2}{(\alpha \mathbf{r}_{ti})^2}}, \quad (1)$$

where  $N$  is the number of the neighbor atoms in the templates;  $\mathbf{r}_{ci}$  and  $\mathbf{r}_{ti}$  are the atomic coordinates in the aligned clusters and template, respectively; and  $\alpha$  is the optimal scaling coefficient of the bond length in the template. A smaller alignment score represents less deviation of the cluster from the template. Each as-extracted cluster from the sample is aligned to both 3661 and 16661 templates, respectively. Figures 3(d) and (e) show the distribution of alignment scores  $f_{3661}$  and  $f_{16661}$  for Sm-centered clusters extracted from the liquid and the as-grown crystal.

In figure 3(d), the score distribution of liquid clusters shows a single peak at (0.19, 0.24) in the  $f_{3661}$ - $f_{16661}$  plane. Both  $f_{3661}$  and  $f_{16661}$  values at the peak position are relatively high, indicating an overall disordered state. On the other hand,  $f_{3661}$  is still significantly smaller than  $f_{16661}$  at the peak position, showing that the undercooled liquid has a more pronounced 3661-type order. This is consistent with our previous analysis [27]. In the as-grown crystal, the clusters are clearly separated into two groups centered at (0.17, 0.10) and (0.12, 0.24) in figure 3(e). These two groups correspond to 3661 and 16661 type clusters, respectively. Using a cut-off value  $f_c = 0.15$  shown as the dash line in the figure, clusters with scores



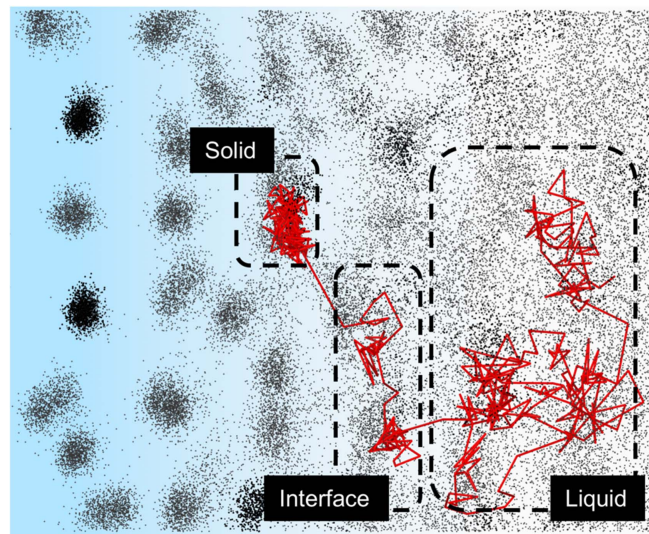


**Figure 4.** A projected trajectory of a Sm atom transiting from liquid to solid during the  $\epsilon$ -Al<sub>60</sub>Sm<sub>11</sub> growth. The atom positions at contiguous time steps are connected. The dots on the background are the surrounding atoms in the whole trajectory.

below 0.15 can be divided into 3661 and 16661 types. In figure 4(f), we plot the populations of each type of clusters as a function of the simulation time. In the initial liquid, while there is no 16661-type clusters,  $\sim 10\%$  Sm centered clusters of the growing part has already formed 3661-type motif, indicating pre-existing 3661-type clusters in the liquid. During the growth process, the number of disordered clusters (alignment scores  $> 0.15$ ) decreases while 3661-type and 16661-type clusters increases. The curves of 3661 and 16661 populations are almost parallel, indicating the two types of local orders are formed in parallel during the growth. The crystallization ends at 225 ns resulting in plateaus on all three curves. During the crystallization process, we can monitor the growth of the crystal by the increase in population of 3661 and 16661 clusters. Knowing the density of these clusters in the crystal, we can convert the slope of time-dependent population increase to interface velocity by  $v = \frac{|k|}{2\rho A}$ , where  $k$  is the slope of the liner fitting in figure 3(f),  $\rho$  is the Sm density in  $\epsilon$ -Al<sub>60</sub>Sm<sub>11</sub> phase and  $A$  is the area of cross section normal to the growth direction. The factor 2 accounts for two interfaces of the crystal slab. We obtained a value of  $0.081 \text{ \AA ns}^{-1}$  for the interface velocity in our simulation.

### 3.3. Dynamical characteristics during the crystallization

In addition to understanding of structural transformation from the localized SRO of liquid structure to the long-range crystalline order, the dynamical characteristics is also important to understand the transformation pathway. In figure 4, we trace the trajectory of a Sm atom when it attaches to the solid from the liquid. When the Sm atom is in the disordered liquid state, it diffuses continuously and the atomic trajectory shows ‘random walk’-like characters. When the atom approaches the  $\epsilon$ -Al<sub>60</sub>Sm<sub>11</sub> phase, the diffusion becomes more localized with occasional jumps at the solid-liquid interface. Eventually, the atom becomes solid-like and only vibrates at the crystalline site.

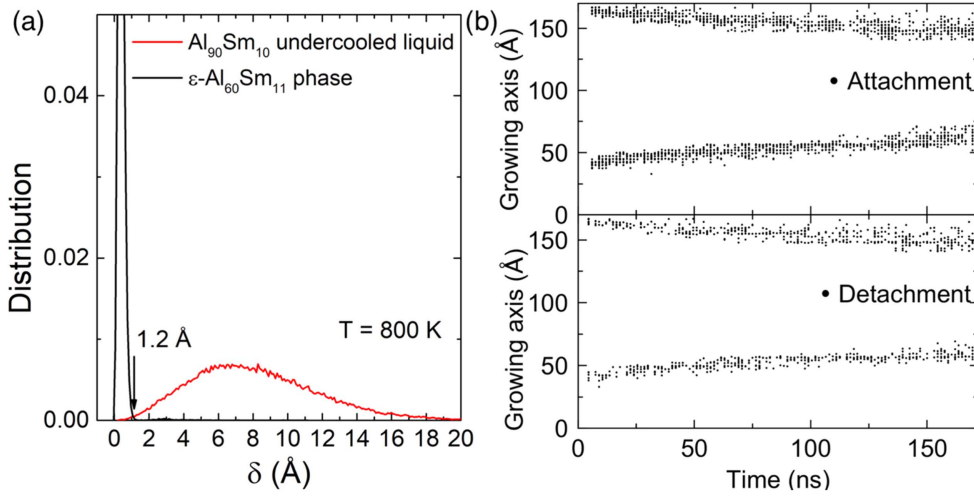


**Figure 5.** (a) The distribution of dynamical order parameter  $\delta$  in the Al-10 at% Sm undercooled liquid and  $\epsilon$ -Al<sub>60</sub>Sm<sub>11</sub> at 800 K. The threshold for labelling an atom either as liquid or as solid is chosen as 1.2 Å which is the crosspoint of the two curves. (b) The time and coordinates of the attachment and detachment events. Only the coordinates at the growing axis are plotted.

Based on the different atom motion in solid and liquid, we employ a dynamical order parameter  $\delta = |\vec{r}(t) - \vec{r}(t - \Delta t)|$  to calculate the displacement that an atom moves within a time interval  $\Delta t$ . Based on this parameter, the attachment and detachment transition between liquid and solid can be well identified with a threshold  $\delta_c$  [30]. Here, a larger sample with 61344 atoms is simulated for better statistical analysis. The threshold is chosen as  $\delta_c = 1.2$  Å with  $\Delta t = 1.5$  ns for Sm atoms according to the dynamical parameter distributions of two phases in figure 5(a). The time and position of the attachment and detachment events are plotted in figure 5(b). Therefore, the attachment rate  $R_a$  and detachment rate  $R_d$ , which is defined as the number of attached/detached atoms in unit time at unit area, can be obtained by averaging all the events during the simulation. Here, we obtained  $R_a = 8.70 \times 10^{-4} \text{ Å}^{-2} \text{ ns}^{-1}$  and  $R_d = 3.83 \times 10^{-4} \text{ Å}^{-2} \text{ ns}^{-1}$ . Based on the attachment/detachment rate, one can also derive the interface velocity with  $v = \frac{|R_a - R_d|}{\rho}$ , where  $\rho$  is the Sm density in the  $\epsilon$ -Al<sub>60</sub>Sm<sub>11</sub> phase. The interface velocity based on the dynamical parameter is  $0.095 \text{ Å ns}^{-1}$ , which is consistent with the interface velocity determined by the structural analysis previously.

#### 4. Conclusion

In summary, using the MD simulations we investigate structural and dynamical evolutions in the polymorphic transformation from the Al-10 at% Sm undercooled liquid to the crystalline  $\epsilon$ -Al<sub>60</sub>Sm<sub>11</sub> phase. The analysis of the PCF and bond angle distribution illustrates similar local atomic arrangements around Al atoms but dramatically different Sm-Sm networking between the liquid and the as-grown crystal structures. A common Sm-centered cluster motif is revealed as a structural precursor in the undercooled liquid. By using the alignment score as the order parameter, we characterized the order development during the crystallization. Moreover, we identified the atomic transformation pathway and obtained atomic attachment/




detachment rates based on atomic motions. The interface velocity is derived consistently by both structural and dynamical order parameters. These results pave the way to a phase-field description for detailed realistic simulations of the devitrification process.

## Acknowledgments

Work at Ames Laboratory was supported by the US Department of Energy, Basic Energy Sciences, Materials Science and Engineering Division, under Contract No. DE-AC02-07CH11358, including a grant of computer time at the National Energy Research Supercomputing Center (NERSC) in Berkeley, CA YS acknowledges support from China Scholarship Council (File No. 201406340015). ZJD acknowledges support from the National Natural Science Foundation of China (No. 11574289). KMH acknowledges support from USTC Qian-Ren B (1000-Talents Program B) fund.

## ORCID iDs

Yang Sun  <https://orcid.org/0000-0002-4344-2920>

Cai-Zhuang Wang  <https://orcid.org/0000-0002-0269-4785>

## References

- [1] Inoue A and Takeuchi A 2004 Recent progress in bulk glassy, nanoquasicrystalline and nanocrystalline alloys *Mater. Sci. Eng. A* **375–377** 16–30
- [2] Brauer S, Ström-Olsen J O, Sutton M, Yang Y S, Zaluska A, Stephenson G B and Köster U 1992 *In situ* x-ray studies of rapid crystallization of amorphous  $\text{NiZr}_2$  *Phys. Rev. B* **45** 7704
- [3] Kalay I, Kramer M J and Napolitano R E 2015 Crystallization kinetics and phase transformation mechanisms in  $\text{Cu}_{56}\text{Zr}_{44}$  glassy alloy *Metall. Mater. Trans. A* **46** 3356–64
- [4] Kramer M J, Margulies L, Goldman A I and Lee P L 2002 Measuring crystal structure dynamics during polymorphic phase transitions *J. Alloys Compd.* **338** 235–41
- [5] Cheng Y Q and Ma E 2011 Atomic-level structure and structure–property relationship in metallic glasses *Prog. Mater. Sci.* **56** 379–473
- [6] Sheng H W, Luo W K, Alamgir F M, Bai J M and Ma E 2006 Atomic packing and short-to-medium-range order in metallic glasses *Nature* **439** 419–25
- [7] Inoue A 1998 Amorphous, nanoquasicrystalline and nanocrystalline alloys in Al-based systems *Prog. Mater. Sci.* **43** 365–520
- [8] Inoue A, Ohtera K, Tao Z and Masumoto T 1988 New amorphous Al–Ln (Ln = Pr, Nd, Sm or Gd) alloys prepared by melt spinning *Japan. J. Appl. Phys.* **27** L1583
- [9] Rizzi P, Baricco M, Borace S and Battezzati L 2001 Phase selection in Al–TM–RE alloys: nanocrystalline Al versus intermetallics *Mater. Sci. Eng. A* **304** 574–8
- [10] Guo J Q, Ohtera K, Kita K, Nagahora J and Kazama N S 1995 Crystallization behavior of  $\text{Al}_{100-x}\text{Sm}_x$  ( $x = 8\text{--}14$  at%) amorphous alloys *Mater. Lett.* **24** 133–8
- [11] Kalay Y E, Chumbley L S and Anderson I E 2008 Crystallization behavior in a highly driven marginal glass forming alloy *J. Non-Cryst. Solids* **354** 3040–8
- [12] Ye Z *et al* 2015 Structural hierarchy as a key to complex phase selection in Al–Sm *Phys. Rev. Mater.* **1** 055601
- [13] Kalay Y E, Yeager C, Chumbley L S, Kramer M J and Anderson I E 2010 Initial crystallization in a nanostructured Al–Sm rare earth alloy *J. Non-Cryst. Solids* **356** 1416–24
- [14] Fang X W, Wang C Z, Yao Y X, Ding Z J and Ho K M 2010 Atomistic cluster alignment method for local order mining in liquids and glasses *Phys. Rev. B* **82** 184204
- [15] Plimpton S 1995 Fast parallel algorithms for short-range molecular dynamics *J. Comput. Phys.* **117** 1–19

- [16] Mendelev M I, Zhang F, Ye Z, Sun Y, Nguyen M C, Wilson S R, Wang C Z and Ho K M 2015 Development of interatomic potentials appropriate for simulation of devitrification of  $\text{Al}_{90}\text{Sm}_{10}$  alloy *Model. Simul. Mater. Sci. Eng.* **23** 45013
- [17] Zhang F, Sun Y, Ye Z, Zhang Y, Wang C-Z, Mendelev M I, Ott R T, Kramer M J, Ding Z-J and Ho K-M 2015 Solute-solute correlations responsible for the prepeak in structure factors of undercooled Al-rich liquids: a molecular dynamics study *J. Phys. Condens. Matter* **27** 205701
- [18] Li M, Wang C-Z, Mendelev M I and Ho K-M 2008 Molecular dynamics investigation of dynamical heterogeneity and local structure in the supercooled liquid and glass states of Al *Phys. Rev. B* **77** 184202
- [19] Jakse N and Pasturel A 2003 Local order of liquid and supercooled zirconium by *ab initio* molecular dynamics *Phys. Rev. Lett.* **91** 195501
- [20] Miracle D B 2004 A structural model for metallic glasses *Nat. Mater.* **3** 697–702
- [21] Liu X J, Xu Y, Hui X, Lu Z P, Li F, Chen G L, Lu J and Liu C T 2010 Metallic liquids and glasses: atomic order and global packing *Phys. Rev. Lett.* **105** 155501
- [22] Royall C P, Williams S R, Ohtsuka T and Tanaka H 2008 Direct observation of a local structural mechanism for dynamic arrest *Nat. Mater.* **7** 556–61
- [23] Coslovich D and Pastore G 2007 Understanding fragility in supercooled Lennard-Jones mixtures: I. Locally preferred structures *J. Chem. Phys.* **127** 124504
- [24] Biroli G, Bouchaud J P, Cavagna A, Grigera T S and Verrocchio P 2008 Thermodynamic signature of growing amorphous order in glass-forming liquids *Nat. Phys.* **4** 771–5
- [25] Hirata A, Guan P, Fujita T, Hirotsu Y, Inoue A, Yavari A R, Sakurai T and Chen M 2011 Direct observation of local atomic order in a metallic glass *Nat. Mater.* **10** 28–33
- [26] Miracle D B, Greer A L and Kelton K F 2008 Icosahedral and dense random cluster packing in metallic glass structures *J. Non. Cryst. Solids* **354** 4049–55
- [27] Sun Y *et al* 2016 ‘Crystal genes’ in metallic liquids and glasses *Sci. Rep.* **6** 23734
- [28] Sun Y, Zhang Y, Zhang F, Ye Z, Ding Z, Wang C Z and Ho K M 2016 Cooling rate dependence of structural order in  $\text{Al}_{90}\text{Sm}_{10}$  metallic glass *J. Appl. Phys.* **120** 15901
- [29] Fang X W, Wang C Z, Hao S G, Kramer M J, Yao Y X, Mendelev M I, Ding Z J, Napolitano R E and Ho K M 2011 Spatially resolved distribution function and the medium-range order in metallic liquid and glass *Sci. Rep.* **1** 194
- [30] Sun Y, Zhang F, Ye Z, Ding Z, Mendelev M I, Kramer M J, Wang C Z and Ho K M 2017 Structural ordering at solid-liquid interfaces in Al–Sm system: a molecular-dynamics study *Mater. Lett.* **186** 26–9